
A Free Lunch in LLM Compression: Revisiting Retraining after Pruning

Moritz Wagner¹ Christophe Roux^{1,2} Max Zimmer^{1,2} Sebastian Pokutta^{1,2}

Abstract

Post-training pruning substantially reduces inference costs but often causes severe quality degradation without adapting the remaining weights. For LLMs, such retraining is commonly considered impractical due to large computational costs, motivating increasingly sophisticated pruning criteria to compensate by selecting better sparsity patterns. In this work, we revisit post-pruning adaptation and study *local reconstruction*: adapting only a small pruned submodel at a time using a small calibration set by matching intermediate activations of the dense model. We conduct a large-scale study across model families and scales (up to 72B parameters) and establish three central results. First, local reconstruction is an effective adaptation mechanism for LLMs, matching post-pruning PEFT while using over an order of magnitude less data and compute. Second, we identify a broad “free lunch” regime in reconstruction *granularity*: across a wide range of submodel sizes, final quality remains essentially unchanged, allowing granularity to be chosen based on memory constraints. Finally, with reconstruction, the pruning criterion becomes less critical: performance gaps between sophisticated methods and simple baselines shrink with model size, making simple methods competitive again. Collectively, our results challenge the prevailing narrative that post-pruning adaptation is impractical for LLMs.

researchers and practitioners. Model compression, particularly post-training pruning, addresses these bottlenecks by identifying and removing redundant weights in pretrained Neural Networks (NNs), yielding *sparse* models with reduced inference costs (Han et al., 2015; Gale et al., 2019; Hoefler et al., 2021).

Historically, post-training pruning has often been performed using a prune-retrain pipeline: remove weights (often by magnitude) and then adapt the remaining weights by retraining them to recover accuracy (Han et al., 2015; Gale et al., 2019; Hoefler et al., 2021). In this work, post-pruning *adaptation* refers to any procedure that adjusts the remaining weights after pruning to recover model quality. For LLMs, full retraining after pruning is viewed as computationally prohibitive since it requires full-model backpropagation, typically on large data volumes, leading to extremely high memory and compute costs (Sun et al., 2024; Frantar & Alistarh, 2023; Zimmer et al., 2025). Magnitude pruning in LLMs can cause large quality drops when the remaining weights are not adapted to compensate for the induced errors (Sun et al., 2024; Yin et al., 2024). As a result, prior work has largely focused on designing better pruning criteria (rules for deciding which weights to remove in each layer) to help ensure the pruned model remains accurate even without post-pruning adaptation.

Such approaches operate *locally*, pruning each weight matrix independently using a small calibration set. Given a single layer with weight matrix $W \in \mathbb{R}^{d_{out} \times d_{in}}$ and calibration input $X \in \mathbb{R}^{d_{in} \times B}$ (obtained by running a small set of sequences containing a total of B tokens through the dense model up to W), the per-matrix pruning objective is

$$\min_{M, \hat{W}} \|WX - (M \odot \hat{W})X\|_F^2, \quad (1)$$

where $\hat{W} \in \mathbb{R}^{d_{out} \times d_{in}}$ is the adapted weight matrix, \odot denotes the elementwise Hadamard product, and $M \in \{0, 1\}^{d_{out} \times d_{in}}$ is a binary pruning mask satisfying some sparsity constraint. Common sparsity constraints are $p\%$ unstructured or $N:M$ semi-structured sparsity (Mishra et al., 2021), where N out of M contiguous weights are kept. The problem given in Equation 1 can be relaxed into two subproblems: (i) *mask selection* chooses M while keeping the weights $\hat{W} = W$ fixed,

1. Introduction

Large Language Models (LLMs) have revolutionized natural language processing with state-of-the-art performance across a wide range of tasks from text generation to code synthesis. However, their scale comes with significant computational and memory demands, posing challenges for both

¹Department for AI in Society, Science, and Technology, Zuse Institute Berlin, Germany ²Institute of Mathematics, Technische Universität Berlin, Germany. Correspondence to: Moritz Wagner <wagner@zib.de>.

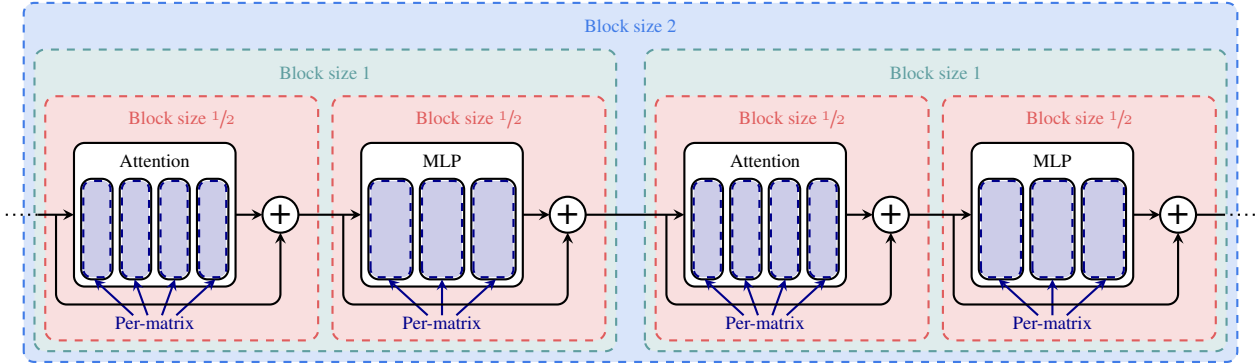


Figure 1. Illustration of reconstruction granularities. At the finest level, *per-matrix* reconstruction adapts each individual weight matrix separately. Block size $1/2$ reconstructs the attention and MLP components of each transformer block independently. Block size 1 reconstructs each full transformer block at a time, and block size 2 reconstructs two consecutive transformer blocks together.

and (ii) *reconstruction* adapts \hat{W} while keeping M fixed. For instance, Wanda (Sun et al., 2024) scores weights by scaling their magnitudes with activation statistics, and does not perform any weight updates, while SparseGPT (Frantar & Alistarh, 2023) additionally performs local weight updates to reduce the resulting reconstruction error. A shared premise across many of these approaches is that strong pruning mask selection is the primary lever, because retraining is infeasible. In this work, we focus on the latter problem of reconstruction, noting that reconstructing a single matrix in isolation is a convex quadratic problem, which admits an analytical solution, and requires significantly less memory compared to retraining the entire model.

More precisely, we revisit post-pruning adaptation and study *local reconstruction* (cf. EBFT by Guo et al., 2024): instead of retraining the full model, we adapt only a small pruned *submodel* (e.g., one transformer block) at a time using a small calibration set by matching intermediate activations of the original dense model. In this work, we distinguish between *reconstruction* (local adaptation using intermediate activations as targets) and *retraining* (adaptation of the entire pruned model using true labels).

Let f be the submodel we want to reconstruct. The local reconstruction objective is given by

$$\min_{\hat{\theta}} \|f(X; \theta) - f(X; M_{\theta} \odot \hat{\theta})\|_2^2, \quad (2)$$

where θ denotes the dense parameters of the submodel, $\hat{\theta}$ the adapted parameters, and M_{θ} the corresponding pruning mask. Because f includes nonlinearities and multiple matrices, it can absorb pruning-induced errors locally (e.g., by compensating across projections within attention and MLP blocks), which is not possible when optimizing a single matrix in isolation.

We study a wide range of such submodel sizes, which we refer to as the *granularity* of reconstruction. Our analysis spans from reconstructing individual weight matrices

to within-block components (reconstructing attention and MLP separately, which we refer to as “block size $1/2$ ”), to full transformer blocks (“block size 1”), and finally to coarser multi-block chunks (cf. Figure 1). By dissecting local reconstruction at different granularities, we make several surprising findings, which we highlight in detail below: (i) local reconstruction makes post-pruning adaptation feasible in regimes where full retraining or Parameter-Efficient Fine-Tuning (PEFT) is not, (ii) we observe a free-lunch regime where reconstructing at smaller granularity reduces peak memory without sacrificing final quality, and (iii) once reconstruction is applied, the apparent advantage of sophisticated pruning criteria shrinks with model size.

Our contributions are summarized as follows. We conduct a large-scale computational study to dissect the design choices for local reconstruction, i.e., the post-pruning adaptation of remaining (non-pruned) weights using a small calibration dataset. Our central findings are:

- 1. Local reconstruction makes adaptation feasible.** Local reconstruction makes post-pruning adaptation practical at LLM scale by restricting optimization to a small submodel at a time, so peak memory scales with the reconstructed submodel rather than the full network. We find that local reconstruction matches Low-Rank Adaptation (LoRA)-based PEFT retraining while using over an order of magnitude less calibration data and compute, making effective adaptation feasible in regimes where full retraining or PEFT is not.
- 2. Local reconstruction admits a free-lunch regime.** Intuitively, increasing the reconstruction granularity should trade quality for resources: coarser granularity should improve final model quality but demand more resources for backpropagation, with full retraining being the most resource-intensive and per-matrix reconstruction the least. However, we find that, across

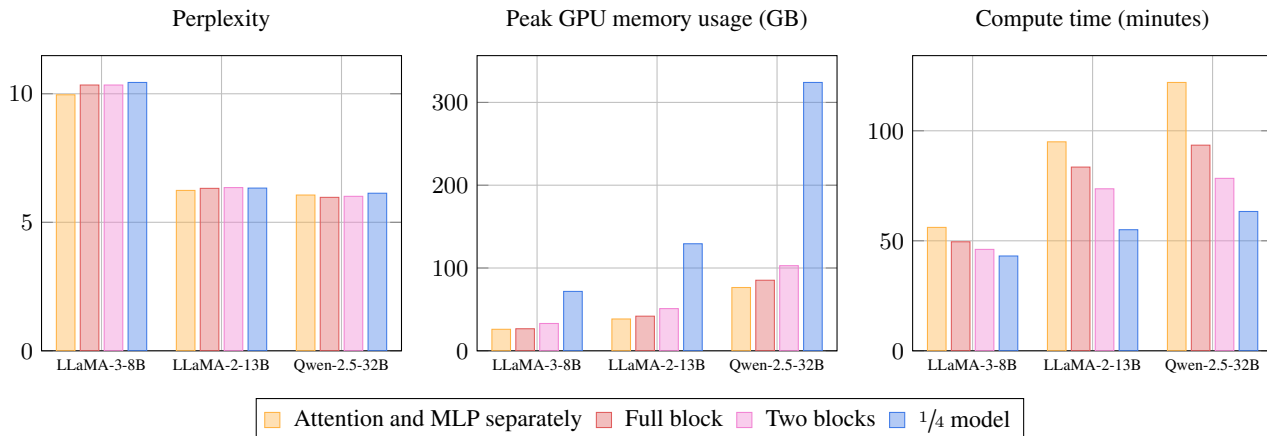


Figure 2. Perplexity and memory usage of three models pruned to 2:4 sparsity with Wanda and reconstructed with different granularities. The number of calibration samples is 1024. $1/4$ of the model is 8, 10, and 16 transformer blocks for LLaMA-3-8B, LLaMA-2-13B, and Qwen-2.5-32B, respectively. We report peak memory as the maximum allocated GPU memory during reconstruction. The compute time is for NVIDIA H100 GPUs. We use as many GPUs as needed to accommodate the reconstruction (at most four GPUs) and do not offload inactive model components.

a wide practical range, increasing the size of the sub-model reconstructed at once does not improve the final model quality. Peak memory usage grows sharply as granularity becomes coarser, while the compute time changes more gradually (cf. Figure 2). This yields a free-lunch regime where granularity can be chosen primarily to satisfy hardware constraints, trading memory for compute time without sacrificing final quality. A surprising exception is per-matrix reconstruction, which consistently underperforms despite being the natural and widely used formulation.

- Mask selection becomes negligible.** With an effective reconstruction step in place, performance gaps between sophisticated pruning criteria and simple baselines shrink with model size, making simple methods increasingly competitive. This is surprising given prior evidence that magnitude pruning is prone to failure in LLMs. Reconstruction largely mitigates this failure, suggesting that part of the apparent advantage of sophisticated mask selection comes from compensating for missing or weak post-pruning adaptation.

Taken together, these findings challenge the prevailing assumption that local post-pruning adaptation is insufficient to recover pruning-induced performance degradation. This renders the prune-retrain pipeline, restricted to a local variant, a practical alternative to avoiding adaptation at LLM scale entirely. Our results further suggest that much of the complexity in recent pruning methods may partially compensate for missing adaptation rather than address fundamental limitations of simpler approaches.

2. Background

Post-training pruning is often studied in a prune-retrain setting: weights are removed and the remaining ones are adapted to recover accuracy. Early work emphasizes iterative procedures and second-order criteria such as Optimal Brain Surgeon (OBS) (LeCun et al., 1989; Hassibi & Stork, 1993), and later work emphasizes iterative prune-retrain schemes for reaching high sparsity and uncovering winning ticket subnetworks (Han et al., 2015; Frankle & Carbin, 2019). For LLMs, full retraining after pruning is considered infeasible in practice due to their large memory and compute footprints and the need for large datasets for re-training. Consequently, much recent work targets settings where post-pruning adaptation is either unnecessary or minimal, making the pruning criterion itself the primary lever. In this regime, magnitude pruning is prone to failure for LLMs. This failure is linked to distinctive activation and weight statistics in LLMs compared to smaller deep learning models such as convolutional NNs (Xiao et al., 2023; Sun et al., 2024; Yin et al., 2024). Dettmers et al. (2022) find that LLMs exhibit outlier features, i.e., features that have significantly larger magnitudes than the other features in the same layer. Intuitively, outlier activations cause a few input directions to dominate a layer’s output, so pruning weights purely by magnitude can remove parameters that are small in absolute value but crucial for preserving those high-activation features, leading to large errors after pruning. This motivates the development of more sophisticated pruning methods that do not rely on full retraining.

Many LLM pruning methods therefore operate *locally* at the level of individual weight matrices using a small calibration set (Sun et al., 2024; Zhang et al., 2024; Frantar & Alistarh, 2023). One line of work focuses on mask se-

lection while keeping the remaining weights fixed: Wanda scores weights using activation statistics (Sun et al., 2024), and RIA further accounts for relative neuron importance (Zhang et al., 2024). A second line *interleaves* mask selection with *per-matrix reconstruction*, updating the surviving weights to reduce activation mismatch on the calibration set. SparseGPT (Frantar & Alistarh, 2023) is a well-established approach in this category, combining OBS-style selection with linear least squares updates; related methods explore alternative optimization strategies for similar per-layer objectives (Zhao et al., 2024; Boža, 2024).

Complementary work emphasizes *post-pruning adaptation* by explicitly updating the remaining weights *after* pruning. The most local variant performs per-matrix reconstruction (with the mask fixed) by minimizing activation error for each linear layer independently as in Equation 1 (Wang et al., 2024). More recent methods reconstruct larger transformer submodels by matching intermediate activations of the dense model as in Equation 2, enabling local error compensation across coupled projections and nonlinearities (Guo et al., 2024; Shin et al., 2024). Related results for quantized vision models suggest that optimizing smaller submodels can outperform full-model calibration under limited calibration data (Li et al., 2021; Jeon et al., 2022).

Another alternative is PEFT after pruning, where a small set of trainable parameters is introduced or selected while most pretrained weights remain frozen (Zimmer et al., 2025; Muñoz et al., 2024). LoRA is a common PEFT mechanism (Hu et al., 2022), and MaskLoRA preserves sparsity by keeping adapters sparse so they can be merged without sacrificing sparsity (Zimmer et al., 2025); related work also studies evolving the pruning mask during fine-tuning (Xiao et al., 2025). See Appendix A for further related work.

Several techniques reduce the memory footprint of fine-tuning without changing the objective, such as activation checkpointing (trading compute for lower activation memory), microbatching with gradient accumulation (reducing peak activations), and PEFT methods such as LoRA (reducing optimizer state and gradient memory but still requiring end-to-end backpropagation through the full model). Local reconstruction is complementary and strictly more modular: by restricting optimization to a small submodel at a time, it allows reconstructing very large models by only loading the active submodel (and its optimizer state) on GPU, while keeping the rest of the network inactive. In contrast, end-to-end fine-tuning and typical PEFT setups generally still require keeping the full model active for the forward and backward pass, making this kind of partial model loading difficult in practice at very large scales. Further, checkpointing or LoRA-style adapters can still be applied within each reconstructed submodel if further savings are needed.

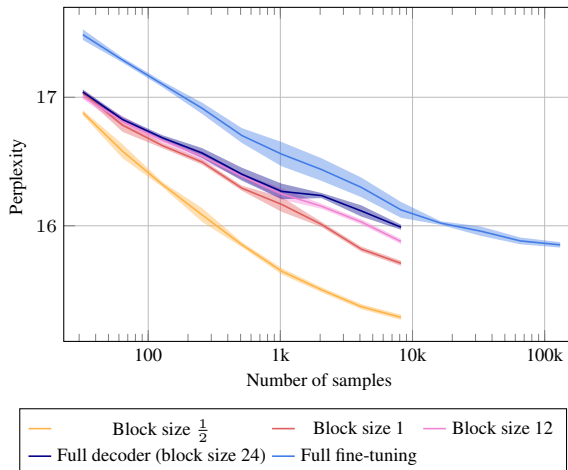


Figure 3. Perplexity of OPT-1.3B pruned to 50% unstructured sparsity with Wanda and reconstructed at different calibration set sizes. The shaded areas indicate the min-max range over random seeds.

3. Experiments

We study post-training pruning and post-pruning adaptation on models from the OPT, LLaMA-2, LLaMA-3, and Qwen-2.5-Instruct families (Zhang et al., 2022; Touvron et al., 2023; Grattafiori et al., 2024; Yang et al., 2024). For pruning and reconstruction, we use calibration data sampled from C4 (Raffel et al., 2020). Each sample is a tokenized text sequence truncated to a length $L = \min(L_{\text{model}}, 4096)$ of tokens, where L_{model} is the model’s maximum context length. We consider both unstructured sparsity and $N:M$ semi-structured patterns. All linear layers except the embedding and LM head are pruned with uniform sparsity following Sun et al. (2024). We evaluate perplexity on WikiText-2 (Merity et al., 2017) and average zero-shot accuracy using the EleutherAI evaluation harness (Gao et al., 2024). The zero-shot accuracy is averaged over the tasks Winogrande (Sakaguchi et al., 2021), GLUE RTE (Wang et al., 2018), OpenBookQA (Mihaylov et al., 2018), BoolQ (Clark et al., 2019), HellaSwag (Zellers et al., 2019), ARC-Easy, and ARC-Challenge (Clark et al., 2018).

We optimize the reconstruction loss given in Equation 2 with AdamW (Loshchilov & Hutter, 2019) with a linear learning rate schedule and a warmup period of 10% of the total number of optimization steps and batch size 2. To compare granularities, we fix the number of epochs per reconstructed submodel, so that each parameter is optimized for the same number of minibatch updates across settings; changing granularity primarily changes which parameters are optimized jointly, rather than how many times any given parameter is updated. For specific hyperparameters, see Appendix G.

There are several design choices regarding the reconstruc-

Table 1. Comparison of local reconstruction (block size 1) and MaskLoRA fine-tuning. The number of calibration samples for pruning is 1024 and the pruning method is Wanda in all cases. ↓: lower is better, ↑: higher is better.

Model	Sparsity Type	Method	Number of Samples	Perplexity ↓	Accuracy ↑	Compute Time	GPU
LLaMA-3-8B	50%	Prune only	-	9.14	56.61%	3 minutes	H200
		Local reconstruction	2048	7.68	58.22%	1.4 hours	H200
		MaskLoRA fine-tuning	131,072	7.70	58.13%	19 hours	H200
Qwen-2.5-7B -Instruct	2:4	Prune only	-	16.01	59.64%	3 minutes	A100 80GB
		Local reconstruction	2048	8.93	64.16%	1.5 hours	A100 80GB
		MaskLoRA fine-tuning	13,1072	8.89	64.02%	196 hours	A100 80GB

tion objective, including the propagation strategy (how calibration data defines inputs and targets) and the loss function (how reconstruction quality is measured). We use MSE as the loss function with activations from the pruned prefix as inputs and activations from the dense model as targets as in Equation 2. Ablations over alternative reconstruction variants using different loss functions and propagation strategies (both inputs and targets from the pruned or dense model) are deferred to Appendix B. We find that the choice of loss function and propagation strategy has no significant impact on the final model quality. Furthermore, Appendix C presents additional experiments investigating the effect of the calibration set on the reconstruction quality, and Appendix D shows how reconstruction affects structured pruning.

Our experiments are organized around four questions: (i) How does local reconstruction compare to retraining (with PEFT) in terms of compute time and hardware requirements? (ii) How does per-matrix reconstruction perform relative to coarser submodel-wise local reconstruction? (iii) Does submodel reconstruction granularity affect final model quality? (iv) After effective reconstruction, how important is the pruning criterion?

(i) How does reconstruction compare to retraining?

A common approach to post-pruning adaptation is retraining the model end-to-end. Since full retraining is prohibitively expensive for LLMs, we apply PEFT to pruned models above 1.3 billion parameters, e.g., the sparsity-preserving LoRA variant MaskLoRA (Zimmer et al., 2025), and only fully fine-tune OPT-1.3B. Table 1 compares local reconstruction (block size 1) to MaskLoRA fine-tuning under two representative settings. On both LLaMA-3-8B and Qwen-2.5-7B-Instruct, local reconstruction achieves essentially the same perplexity and accuracy as MaskLoRA while using 64× fewer samples. For LLaMA-3-8B, this leads to a 13.6× speedup, while for Qwen-2.5-7B-Instruct, it leads to a 130× speedup. Figure 3 shows that, at equal calibration set sizes, local reconstruction achieves much lower perplexity than full fine-tuning on OPT-1.3B. Even when increasing the calibration set size to 131k samples, full fine-tuning OPT-1.3B yields higher perplexity than reconstruction with block size $\frac{1}{2}$ and 1024 samples (15.85 vs. 15.60 perplexity).

Table 2. Per-matrix vs. block size 1 local reconstruction for multiple models pruned to 2:4 and 60% unstructured sparsity. The number of calibration samples for pruning is 256 and the pruning method is Wanda. The best result for each model and sparsity type combination is highlighted in bold. ↓: lower is better, ↑: higher is better.

Model	Sparsity	Accuracy (in %) ↑		Perplexity ↓	
		Per-matrix	Block Size 1	Per-matrix	Block Size 1
OPT-6.7B	2:4	47.02	48.98	14.25	12.70
LLaMA-2-13B		54.15	56.49	7.59	6.22
LLaMA-2-70B		63.14	63.84	5.01	4.56
Qwen-2.5-14B		64.49	65.68	58.58	12.85
Qwen-2.5-32B		67.10	67.39	13.89	6.50
Qwen-2.5-72B		69.99	69.94	5.96	5.86
OPT-6.7B	60%	44.31	46.94	15.76	13.22
LLaMA-2-13B		56.43	58.02	7.22	6.21
LLaMA-2-70B		63.81	63.98	4.72	4.52
Qwen-2.5-14B		64.66	65.30	76.10	9.23
Qwen-2.5-32B		66.29	67.30	7.02	6.28
Qwen-2.5-72B		69.78	70.18	5.68	5.70

These results underscore a practical advantage of local reconstruction: **Fine-tuning a pruned model end-to-end requires orders of magnitude more data and hence substantially more compute to achieve the same final model performance.** Moreover, local reconstruction can be performed in a memory-constrained setting. For example, a 32B model can be locally reconstructed on a single 80GB H100 without gradient checkpointing, offloading inactive model components, or quantization. Sparsity-preserving LoRA variants such as MaskLoRA, on the other hand, need the masked low-rank adapter matrices for the backward pass and hence require gradient checkpointing when applied to larger models (without gradient checkpointing, MaskLoRA fine-tuning of Qwen-2.5-32B with the settings detailed in Appendix G requires 275GB of GPU memory).

(ii) How does per-matrix reconstruction compare?

Table 2 compares per-matrix reconstruction to local reconstruction at the granularity of full transformer blocks (block size 1) when pruning with Wanda. Overall, the pattern is consistent: **Across models and sparsities, per-matrix reconstruction underperforms compared to block-wise reconstruction.** It almost always yields worse perplexity and zero-shot accuracy than block-wise reconstruction, often by

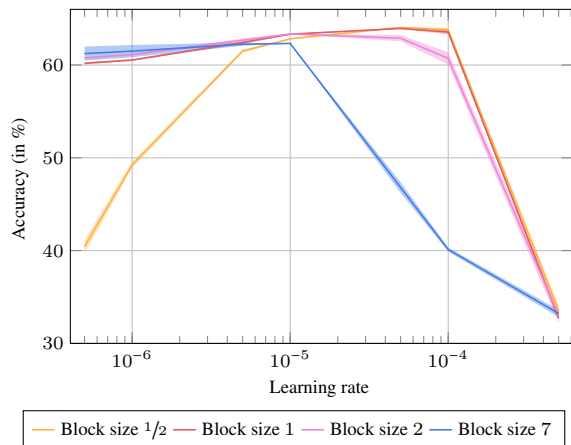


Figure 4. Average zero-shot accuracy of Qwen-2.5-7B-Instruct pruned to 2:4 sparsity and reconstructed at different granularities and learning rates. The number of calibration samples for pruning is 1024 and the pruning method is Wanda. The shaded areas indicate the min-max range over random seeds.

a clear margin. This trend holds across additional models and pruning methods beyond Wanda; the corresponding results are reported in Appendix E and Appendix F. Interestingly, the per-matrix vs. block-wise gap tends to shrink with model scale and at 72B parameters it becomes negligible. This pattern indicates that at sufficiently large model scales, individual matrices provide enough capacity for per-matrix reconstruction to be competitive. This is particularly encouraging in the regime where models are so large that block-wise reconstruction becomes difficult on limited hardware: per-matrix reconstruction can then serve as a viable, more memory-efficient option without a performance penalty.

For smaller models and under high sparsity levels the remaining weights of an individual matrix might not provide enough degrees of freedom to match the dense output well across the feature space: improving the fit along one set of directions can come at the expense of others, leaving little room to “hide” errors. In contrast, reconstructing a nonlinear submodel such as an MLP provides substantially more flexibility through multiple coupled matrices and nonlinearities, allowing errors to be redistributed and locally compensated. Empirically, we find that moving from per-matrix reconstruction to within-block reconstruction (block size 1/2) already reaches the capacity needed to fit the calibration data well (see Appendix E).

(iii) Does granularity affect final model quality?

Table 3 compares reconstruction at different granularities for multiple models and sparsity types. From separate reconstruction of attention and MLP components to reconstruction of a quarter of the model at once, perplexity and zero-shot accuracy are very similar and the differences

Table 3. Perplexity and zero-shot accuracy of three different models pruned to 50% unstructured and 2:4 sparsity and reconstructed at different granularities. The number of calibration samples for pruning is 1024 and the pruning method is Wanda. The results are averaged over multiple random seeds. The best result for each model and sparsity type combination is highlighted in bold. ↓: lower is better, ↑: higher is better.

Model Dense PPL	Block Size	Perplexity ↓		Accuracy (in %) ↑	
		Unstructured	2:4	Unstructured	2:4
LLaMA-3-8B 5.83	No rec.	8.96	21.85	56.89	45.67
	1/2	7.79	10.24	59.77	55.23
	1	7.72	10.31	58.67	54.44
	2	7.75	10.32	58.36	52.72
	8	7.89	10.53	57.90	52.87
LLaMA-2-13B 4.57	No rec.	5.54	8.39	60.25	53.23
	1/2	5.25	6.22	61.14	58.77
	1	5.25	6.29	61.43	58.65
	2	5.27	6.35	60.86	57.84
	10	5.28	6.32	61.06	57.11
Qwen-2.5-32B 4.90	No rec.	6.09	8.00	68.03	66.41
	1/2	5.93	6.06	69.05	68.79
	1	5.92	5.97	69.18	69.06
	2	5.98	6.01	69.15	69.19
	16	5.97	6.13	69.09	69.05

are small relative to the overall prune-to-reconstruct gains. For LLaMA-3-8B and OPT-1.3B (Figure 3), more coarse-grained reconstruction even tends to perform worse. This trend coincides with the findings of Li et al. (2021), that more coarse-grained local reconstruction of quantized vision models tends to perform worse. However, we do not find this effect continues to hold for models above 8 billion parameters. More detailed results are reported in Appendix E.

Taken together, these results show a surprising insight: one might expect coarser reconstruction, and ultimately full end-to-end fine-tuning, to yield the best quality, since it can coordinate updates across more parameters and nonlinearities (albeit at higher compute and memory cost), however, this is not what we observe. **The final model quality is largely insensitive to granularity.** An exception is per-matrix reconstruction, which consistently underperforms (cf. (ii)). Hence, granularity should be chosen primarily for feasibility: since quality is largely insensitive to how much of the model is reconstructed at once, we can trade memory for compute by using smaller reconstructed submodels. Figure 2 shows how peak memory usage increases sharply with granularity while the final perplexity stays flat, whereas compute time changes more gradually with granularity. This creates a free-lunch scenario where we can choose a granularity that enables reconstruction on given hardware while model quality is not impacted by this choice; the only trade-off is compute time. In practice, the learning-rate choice is similarly stable across fine-grained settings, and only needs a slightly smaller value for very coarse-grained reconstruction (see Figure 4).

Table 4. Magnitude pruning vs. Wanda and SparseGPT. The models are pruned to 2:4 sparsity and reconstructed with block size 1 and 256 calibration samples. The best result for each model is highlighted in bold. ↓: lower is better, ↑: higher is better.

Model	Accuracy (in %) ↑						Perplexity ↓					
	No Reconstruction			Reconstruction			No Reconstruction			Reconstruction		
	Magnitude	Wanda	SparseGPT	Magnitude	Wanda	SparseGPT	Magnitude	Wanda	SparseGPT	Magnitude	Wanda	SparseGPT
Qwen-2.5-0.5B	33.28	36.76	38.53	39.25	43.08	42.85	21017.80	65.86	28.16	31.35	20.48	19.54
Qwen-2.5-3B	32.28	48.31	52.90	51.31	55.29	55.38	27844.06	22.10	16.17	23.07	12.59	12.92
LLaMA-2-7B	47.47	48.61	51.57	49.02	52.36	52.97	36.09	9.90	9.14	10.06	6.98	7.01
Qwen-2.5-7B	41.23	59.18	60.81	61.52	61.52	61.63	5974.84	15.98	13.02	10.18	9.60	9.69
LLaMA-2-13B	49.85	53.67	55.92	53.46	56.49	57.86	7.37	7.71	7.62	7.04	6.22	6.39
Qwen-2.5-14B	53.83	63.75	64.76	65.02	65.68	65.63	1424.70	242.79	198.16	12.11	12.85	10.87
Qwen-2.5-32B	58.55	66.41	66.33	67.32	67.39	67.26	38.34	37.52	7.11	6.31	6.50	6.71
LLaMA-2-70B	58.87	62.86	62.47	63.12	63.84	63.67	6.23	5.02	5.22	4.60	4.56	4.79
Qwen-2.5-72B	51.07	69.31	69.20	69.03	69.94	69.44	226.30	5.99	6.83	5.93	5.86	6.39

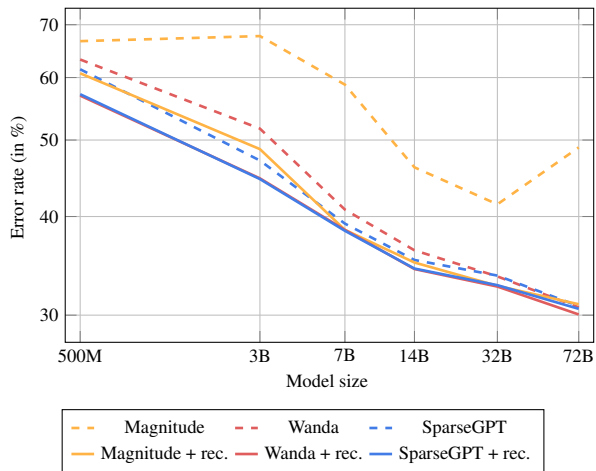


Figure 5. Average zero-shot error rate (1 - accuracy) vs. model size for Qwen-2.5 Instruct models when pruned to 2:4 sparsity. The number of calibration samples is 256 and the pruning method is Wanda. Both axes are on a log scale.

(iv) How important is the pruning criterion after reconstruction?

We now analyze how much the pruning criterion matters once local reconstruction is applied. Table 4 highlights a premise that has shaped much recent LLM pruning work: if post-pruning adaptation is assumed infeasible, then mask selection is the primary lever, and we indeed observe large gaps between magnitude pruning and stronger criteria such as Wanda and SparseGPT in the *No Reconstruction* columns. This explains why increasingly sophisticated mask-selection rules have been a central focus: without reconstruction, their effect is large. The *Reconstruction* columns show a different story. **Once we do allow a post-pruning adaptation step, much of the pruning-induced error can be absorbed, and the performance differences between pruning criteria disappear with increasing model size.**

This reduced dependence on the pruning criterion is especially pronounced at larger scales. Figure 5 visualizes that reconstruction largely closes the accuracy gap between magni-

tude pruning and more sophisticated criteria as model size increases, and in some cases magnitude pruning even matches or slightly surpasses SparseGPT after reconstruction. Additionally, Figure 5 shows that Wanda and SparseGPT are essentially equivalent in terms of zero-shot accuracy after reconstruction, while there is a clear gap without reconstruction.

Overall, these results suggest that part of the apparent advantage of sophisticated pruning criteria without reconstruction comes from compensating for missing post-pruning adaptation; once a strong reconstruction step is in place, the choice of pruning criterion becomes a secondary consideration at scale.

4. Conclusion

We revisit the prune-retrain paradigm for LLMs with a focus on *local reconstruction*, which adapts small pruned submodels by matching intermediate activations of the original dense model, and we conduct a large-scale evaluation across model families and sizes.

Our results support three main findings. First, local reconstruction is not merely a cheap approximation to end-to-end fine-tuning: it matches and sometimes surpasses full fine-tuning and LoRA-style baselines, while operating in a substantially cheaper data and compute regime. Second, reconstruction granularity admits a broad free-lunch regime: beyond per-matrix reconstruction (which is consistently worse), final perplexity and zero-shot accuracy are largely insensitive to how much of the model is reconstructed at once, even though peak memory varies sharply; granularity should therefore be chosen primarily based on hardware constraints rather than expected quality gains. Third, effective reconstruction changes the role of mask selection: after reconstruction, performance gaps between pruning criteria disappear with increasing model scale, making simple baselines increasingly competitive at larger sizes.

Together, these findings challenge the “avoid retraining at all costs” narrative in LLM pruning. When done properly, local

post-pruning reconstruction is not a second-best fallback but a strong default: it can rival PEFT and full fine-tuning while being feasible at model scales where these end-to-end adaptation methods are simply too expensive, and it shifts the focus from more elaborate mask-selection rules toward efficient, well-configured reconstruction.

Acknowledgements

This research was partially supported by the DFG Cluster of Excellence MATH+ (EXC-2046/2, project id 390685689) funded by the Deutsche Forschungsgemeinschaft (DFG) as well as by the German Federal Ministry of Research, Technology and Space (research campus Modal, fund number 05M14ZAM, 05M20ZBM) and the VDI/VDE Innovation + Technik GmbH (fund number 16IS23025B).

References

- An, Y., Zhao, X., Yu, T., Tang, M., and Wang, J. Fluctuation-based adaptive structured pruning for large language models. In *Proceedings of the AAAI Conference on Artificial Intelligence*, volume 38, pp. 10865–10873, 2024. URL <https://ojs.aaai.org/index.php/AAAI/article/view/28960/29826>.
- Bellec, G., Kappel, D., Maass, W., and Legenstein, R. Deep rewiring: Training very sparse deep networks. November 2018. URL https://openreview.net/forum?id=BJ_wN01C-.
- Boža, V. Fast and effective weight update for pruned large language models. *Transactions on Machine Learning Research*, 2024. URL <https://openreview.net/forum?id=1hcxpXd9Jir>.
- Clark, C., Lee, K., Chang, M.-W., Kwiatkowski, T., 0001, M. C., and Toutanova, K. Boolq: Exploring the surprising difficulty of natural yes/no questions. *NAACL-HLT*, pp. 2924–2936, May 2019. doi: 10.18653/v1/n19-1300. URL <https://doi.org/10.18653/v1/n19-1300>.
- Clark, P., Cowhey, I., Etzioni, O., Khot, T., Sabharwal, A., Schoenick, C., and Tafjord, O. Think you have solved question answering? try arc, the ai2 reasoning challenge. *CoRR*, abs/1803.05457, March 2018. URL <http://arxiv.org/abs/1803.05457>.
- Dettmers, T. and Zettlemoyer, L. Sparse networks from scratch: Faster training without losing performance. *CoRR*, abs/1907.04840, July 2019. URL <http://arxiv.org/abs/1907.04840>.
- Dettmers, T., Lewis, M., Belkada, Y., and Zettlemoyer, L. Llm.int8(): 8-bit matrix multiplication for transformers at scale. *CoRR*, abs/2208.07339, 2022. doi: 10.48550/arxiv.2208.07339. URL <https://doi.org/10.48550/arxiv.2208.07339>.
- Evci, U., Gale, T., Menick, J., Castro, P. S., and Elsen, E. Rigging the lottery: Making all tickets winners. In III, H. D. and Singh, A. (eds.), *Proceedings of the 37th International Conference on Machine Learning*, volume 119 of *Proceedings of Machine Learning Research*, pp. 2943–2952. PMLR, 13–18 Jul 2020. URL <https://proceedings.mlr.press/v119/evci20a.html>.
- Frankle, J. and Carbin, M. The lottery ticket hypothesis: Finding sparse, trainable neural networks. In *International Conference on Learning Representations*, 2019. URL <https://openreview.net/forum?id=rJl-b3RcF7>.
- Frantar, E. and Alistarh, D. Sparsegpt: Massive language models can be accurately pruned in one-shot. In *International Conference on Machine Learning*, pp. 10323–10337. PMLR, 2023. URL <https://proceedings.mlr.press/v202/frantar23a/frantar23a.pdf>.
- Gale, T., Elsen, E., and Hooker, S. The state of sparsity in deep neural networks. *CoRR*, abs/1902.09574, 2019. URL <http://arxiv.org/abs/1902.09574>.
- Gao, L., Tow, J., Abbasi, B., Biderman, S., Black, S., DiPofi, A., Foster, C., Golding, L., Hsu, J., Le Noac’h, A., Li, H., McDonell, K., Muennighoff, N., Ociepa, C., Phang, J., Reynolds, L., Schoelkopf, H., Skowron, A., Sutawika, L., Tang, E., Thite, A., Wang, B., Wang, K., and Zou, A. The language model evaluation harness, 07 2024.
- Grattafiori, A., Dubey, A., Jauhri, A., Pandey, A., Kadian, A., Al-Dahle, A., Letman, A., Mathur, A., Schelten, A., Vaughan, A., Yang, A., Fan, A., Goyal, A., Hartshorn, A., Yang, A., Mitra, A., Sravankumar, A., Korenev, A., Hinsvark, A., Rao, A., Zhang, A., Rodriguez, A., Gregerson, A., Spataru, A., Roziere, B., Biron, B., Tang, B., Chern, B., Caucheteux, C., Nayak, C., Bi, C., Marra, C., McConnell, C., Keller, C., Touret, C., Wu, C., Wong, C., Ferrer, C. C., Nikolaidis, C., Allonsius, D., Song, D., Pintz, D., Livshits, D., Wyatt, D., Esiobu, D., Choudhary, D., Mahajan, D., Garcia-Olano, D., Perino, D., Hupkes, D., Lakomkin, E., AlBadawy, E., Lobanova, E., Dinan, E., Smith, E. M., Radenovic, F., Guzmán, F., Zhang, F., Synnaeve, G., Lee, G., Anderson, G. L., Thattai, G., Nail, G., Mialon, G., Pang, G., Cucurell, G., Nguyen, H., Korevaar, H., Xu, H., Touvron, H., Zarov, I., Ibarra, I. A., Kloumann, I., Misra, I., Evtimov, I., Zhang, J., Copet, J., Lee, J., Geffert, J., Vranes, J., Park, J., Mahadeokar, J., Shah, J., van der Linde, J., Billock, J., Hong, J., Lee, J., Fu, J., Chi, J., Huang, J., Liu, J., Wang, J., Yu, J., Bitton, J., Spisak, J., Park, J., Rocca, J., Johnstun, J., Saxe, J., Jia,

J., Alwala, K. V., Prasad, K., Upasani, K., Plawiak, K., Li, K., Heafield, K., Stone, K., El-Arini, K., Iyer, K., Malik, K., Chiu, K., Bhalla, K., Lakhota, K., Rantala-Yearly, L., van der Maaten, L., Chen, L., Tan, L., Jenkins, L., Martin, L., Madaan, L., Malo, L., Blecher, L., Landzaat, L., de Oliveira, L., Muzzi, M., Pasupuleti, M., Singh, M., Paluri, M., Kardas, M., Tsimpoukelli, M., Oldham, M., Rita, M., Pavlova, M., Kambadur, M., Lewis, M., Si, M., Singh, M. K., Hassan, M., Goyal, N., Torabi, N., Bashlykov, N., Bogoychev, N., Chatterji, N., Zhang, N., Duchenne, O., Çelebi, O., Alrassy, P., Zhang, P., Li, P., Vasic, P., Weng, P., Bhargava, P., Dubal, P., Krishnan, P., Koura, P. S., Xu, P., He, Q., Dong, Q., Srinivasan, R., Ganapathy, R., Calderer, R., Cabral, R. S., Stojnic, R., Raileanu, R., Maheswari, R., Girdhar, R., Patel, R., Sauvestre, R., Polidoro, R., Sumbaly, R., Taylor, R., Silva, R., Hou, R., Wang, R., Hosseini, S., Chennabasappa, S., Singh, S., Bell, S., Kim, S. S., Edunov, S., Nie, S., Narang, S., Raparthy, S., Shen, S., Wan, S., Bhosale, S., Zhang, S., Vandenhende, S., Batra, S., Whitman, S., Sootla, S., Collot, S., Gururangan, S., Borodinsky, S., Herman, T., Fowler, T., Sheasha, T., Georgiou, T., Scialom, T., Speckbacher, T., Mihaylov, T., Xiao, T., Karn, U., Goswami, V., Gupta, V., Ramanathan, V., Kerkez, V., Gonguet, V., Do, V., Vogeti, V., Albiero, V., Petrovic, V., Chu, W., Xiong, W., Fu, W., Meers, W., Martinet, X., Wang, X., Wang, X., Tan, X. E., Xia, X., Xie, X., Jia, X., Wang, X., Goldschlag, Y., Gaur, Y., Babaei, Y., Wen, Y., Song, Y., Zhang, Y., Li, Y., Mao, Y., Coudert, Z. D., Yan, Z., Chen, Z., Papakipos, Z., Singh, A., Srivastava, A., Jain, A., Kelsey, A., Shajnfeld, A., Gangidi, A., Victoria, A., Goldstand, A., Menon, A., Sharma, A., Boesenberg, A., Baevski, A., Feinstein, A., Kallet, A., Sangani, A., Teo, A., Yunus, A., Lupu, A., Alvarado, A., Caples, A., Gu, A., Ho, A., Poulton, A., Ryan, A., Ramchandani, A., Dong, A., Franco, A., Goyal, A., Saraf, A., Chowdhury, A., Gabriel, A., Bharambe, A., Eisenman, A., Yazdan, A., James, B., Maurer, B., Leonhardi, B., Huang, B., Loyd, B., Paola, B. D., Paranjape, B., Liu, B., Wu, B., Ni, B., Hancock, B., Wasti, B., Spence, B., Stojkovic, B., Gamido, B., Montalvo, B., Parker, C., Burton, C., Mejia, C., Liu, C., Wang, C., Kim, C., Zhou, C., Hu, C., Chu, C.-H., Cai, C., Tindal, C., Feichtenhofer, C., Gao, C., Civin, D., Beaty, D., Kreymer, D., Li, D., Adkins, D., Xu, D., Testuggine, D., David, D., Parikh, D., Liskovich, D., Foss, D., Wang, D., Le, D., Holland, D., Dowling, E., Jamil, E., Montgomery, E., Presani, E., Hahn, E., Wood, E., Le, E.-T., Brinkman, E., Arcaute, E., Dunbar, E., Smothers, E., Sun, F., Kreuk, F., Tian, F., Kokkinos, F., Ozgenel, F., Caggioni, F., Kanayet, F., Seide, F., Florez, G. M., Schwarz, G., Badeer, G., Swee, G., Halpern, G., Herman, G., Sizov, G., Guangyi, Zhang, Lakshminarayanan, G., Inan, H., Shojanazeri, H., Zou, H., Wang, H., Zha, H., Habeeb, H., Rudolph, H., Suk, H., Aspegren, H., Goldman, H., Zhan,

H., Damlaj, I., Molybog, I., Tufanov, I., Leontiadis, I., Veliche, I.-E., Gat, I., Weissman, J., Geboski, J., Kohli, J., Lam, J., Asher, J., Gaya, J.-B., Marcus, J., Tang, J., Chan, J., Zhen, J., Reizenstein, J., Teboul, J., Zhong, J., Jin, J., Yang, J., Cummings, J., Carvill, J., Shepard, J., McPhie, J., Torres, J., Ginsburg, J., Wang, J., Wu, K., U, K. H., Saxena, K., Khandelwal, K., Zand, K., Matosich, K., Veeraraghavan, K., Michelena, K., Li, K., Jagadeesh, K., Huang, K., Chawla, K., Huang, K., Chen, L., Garg, L., A, L., Silva, L., Bell, L., Zhang, L., Guo, L., Yu, L., Moshkovich, L., Wehrstedt, L., Khabsa, M., Avalani, M., Bhatt, M., Mankus, M., Hasson, M., Lennie, M., Reso, M., Groshev, M., Naumov, M., Lathi, M., Keneally, M., Liu, M., Seltzer, M. L., Valko, M., Restrepo, M., Patel, M., Vyatskov, M., Samvelyan, M., Clark, M., Macey, M., Wang, M., Hermoso, M. J., Metanat, M., Rastegari, M., Bansal, M., Santhanam, N., Parks, N., White, N., Bawa, N., Singhal, N., Egebo, N., Usunier, N., Mehta, N., Laptev, N. P., Dong, N., Cheng, N., Chernoguz, O., Hart, O., Salpekar, O., Kalinli, O., Kent, P., Parekh, P., Saab, P., Balaji, P., Rittner, P., Bontrager, P., Roux, P., Dollar, P., Zvyagina, P., Ratanchandani, P., Yuvraj, P., Liang, Q., Alao, R., Rodriguez, R., Ayub, R., Murthy, R., Nayani, R., Mitra, R., Parthasarathy, R., Li, R., Hogan, R., Battey, R., Wang, R., Howes, R., Rinott, R., Mehta, S., Siby, S., Bondu, S. J., Datta, S., Chugh, S., Hunt, S., Dhillon, S., Sidorov, S., Pan, S., Mahajan, S., Verma, S., Yamamoto, S., Ramaswamy, S., Lindsay, S., Lindsay, S., Feng, S., Lin, S., Zha, S. C., Patil, S., Shankar, S., Zhang, S., Zhang, S., Wang, S., Agarwal, S., Sajuyigbe, S., Chintala, S., Max, S., Chen, S., Kehoe, S., Satterfield, S., Govindaprasad, S., Gupta, S., Deng, S., Cho, S., Virk, S., Subramanian, S., Choudhury, S., Goldman, S., Remez, T., Glaser, T., Best, T., Koehler, T., Robinson, T., Li, T., Zhang, T., Matthews, T., Chou, T., Shaked, T., Vontimitta, V., Ajayi, V., Montanez, V., Mohan, V., Kumar, V. S., Mangla, V., Ionescu, V., Poenaru, V., Mihailescu, V. T., Ivanov, V., Li, W., Wang, W., Jiang, W., Bouaziz, W., Constable, W., Tang, X., Wu, X., Wang, X., Wu, X., Gao, X., Kleinman, Y., Chen, Y., Hu, Y., Jia, Y., Qi, Y., Li, Y., Zhang, Y., Zhang, Y., Adi, Y., Nam, Y., Yu, Wang, Zhao, Y., Hao, Y., Qian, Y., Li, Y., He, Y., Rait, Z., DeVito, Z., Rosnbrick, Z., Wen, Z., Yang, Z., Zhao, Z., and Ma, Z. The llama 3 herd of models. July 2024. URL <https://arxiv.org/abs/2407.21783>.

Guo, S., Wu, F., Zhang, L., Zheng, X., Zhang, S., Chao, F., Shi, Y., and Ji, R. Ebf: Effective and block-wise fine-tuning for sparse llms. *CoRR*, abs/2402.12419, 2024. URL <https://openreview.net/forum?id=oUj1HbMhvX>.

Han, S., Pool, J., Tran, J., and Dally, W. Learning both weights and connections for efficient neural networks. In Cortes, C., Lawrence, N., Lee, D., Sugiyama, M.,

- and Garnett, R. (eds.), *Advances in Neural Information Processing Systems*, volume 28. Curran Associates, Inc., 2015. URL https://proceedings.neurips.cc/paper_files/paper/2015/file/ae0eb3eed39d2bcef4622b2499a05fe6-Paper.pdf.
- Hassibi, B. and Stork, D. Second order derivatives for network pruning: Optimal brain surgeon. In Hanson, S., Cowan, J., and Giles, C. (eds.), *Advances in Neural Information Processing Systems*, volume 5. Morgan-Kaufmann, 1993. URL <https://proceedings.neurips.cc/paper/1992/file/303ed4c69846ab36c2904d3ba8573050-Paper.pdf>.
- Hoefler, T., Alistarh, D., Ben-Nun, T., Dryden, N., and Peste, A. Sparsity in deep learning: Pruning and growth for efficient inference and training in neural networks. *Journal of Machine Learning Research*, 22(241):1–124, 2021. URL <http://jmlr.org/papers/v22/21-0366.html>.
- Hu, E. J., yelong shen, Wallis, P., Allen-Zhu, Z., Li, Y., Wang, S., Wang, L., and Chen, W. LoRA: Low-rank adaptation of large language models. In *International Conference on Learning Representations*, 2022. URL <https://openreview.net/forum?id=nZevKeeFYf9>.
- Jeon, Y., Lee, C., Cho, E., and Ro, Y. Mr. biq: Post-training non-uniform quantization based on minimizing the reconstruction error. In *Proceedings of the IEEE/CVF conference on computer vision and pattern recognition*, pp. 12329–12338, 2022. URL https://openaccess.thecvf.com/content/CVPR2022/papers/Jeon_Mr.BiQ_Post-Training_Non-Uniform_Quantization_Based_on_Minimizing_the_Reconstruction_Error_CVPR_2022_paper.pdf.
- Kaddour, J. The minipile challenge for data-efficient language models. *CoRR*, abs/2304.08442, 2023. doi: 10.48550/arxiv.2304.08442. URL <https://doi.org/10.48550/arxiv.2304.08442>.
- LeCun, Y., Denker, J. S., and Solla, S. A. Optimal brain damage. In Touretzky, D. S. (ed.), *Advances in Neural Information Processing Systems 2, [NIPS Conference, Denver, Colorado, USA, November 27-30, 1989]*, pp. 598–605. Morgan Kaufmann, 1989. URL <http://papers.nips.cc/paper/250-optimal-brain-damage>.
- Li, Y., Gong, R., Tan, X., Yang, Y., Hu, P., Zhang, Q., Yu, F., Wang, W., and Gu, S. Brecq: Pushing the limit of post-training quantization by block reconstruction. *International Conference on Learning Representations*, 2021. URL <https://openreview.net/forum?id=POWv6hDd9XH>.
- Liu, S., Van der Lee, T., Yaman, A., Atashgahi, Z., Ferraro, D., Sokar, G., Pechenizkiy, M., and Mocanu, D. C. Topological insights into sparse neural networks. pp. 279–294, 2020.
- Loshchilov, I. and Hutter, F. Decoupled weight decay regularization. In *International Conference on Learning Representations*, 2019. URL <https://openreview.net/forum?id=Bkg6RiCqY7>.
- Merity, S., Xiong, C., Bradbury, J., and Socher, R. Pointer sentinel mixture models, 2017. URL <https://openreview.net/forum?id=Byj72udxe>.
- Mihaylov, T., Clark, P., Khot, T., and Sabharwal, A. Can a suit of armor conduct electricity? a new dataset for open book question answering. *EMNLP*, pp. 2381–2391, September 2018. doi: 10.18653/v1/d18-1260. URL <https://doi.org/10.18653/v1/d18-1260>.
- Mishra, A. K., Latorre, J. A., Pool, J., Stosic, D., Stosic, D., Venkatesh, G., Yu, C., and Micikevicius, P. Accelerating sparse deep neural networks. *CoRR*, abs/2104.08378, April 2021. URL <https://arxiv.org/abs/2104.08378>.
- Mocanu, D. C., Mocanu, E., Stone, P., Nguyen, P. H., Gibescu, M., and Liotta, A. Scalable training of artificial neural networks with adaptive sparse connectivity inspired by network science. *Nature Communications*, 9(1), June 2018. doi: 10.1038/s41467-018-04316-3.
- Mostafa, H. and Wang, X. Parameter efficient training of deep convolutional neural networks by dynamic sparse reparameterization. pp. 4646–4655, 2019. URL <https://proceedings.mlr.press/v97/mostafal9a/mostafal9a.pdf>.
- Muñoz, J. P., Yuan, J., and Jain, N. Sqft: Low-cost model adaptation in low-precision sparse foundation models. *EMNLP*, pp. 12817–12832, October 2024. doi: 10.18653/v1/2024.findings-emnlp.749. URL <https://doi.org/10.18653/v1/2024.findings-emnlp.749>.
- Raffel, C., Shazeer, N., Roberts, A., Lee, K., Narang, S., Matena, M., Zhou, Y., Li, W., and Liu, P. J. Exploring the limits of transfer learning with a unified text-to-text transformer. *Journal of Machine Learning Research*, 21(140):1–67, 2020. URL <https://www.jmlr.org/papers/volume21/20-074/20-074.pdf>.
- Sakaguchi, K., Bras, R. L., Bhagavatula, C., and Choi, Y. Winogrande: An adversarial winograd schema challenge at scale. *Communications of the ACM*, 64(9):99–106, 2021.

- Shin, S., Park, W., Lee, J., and Lee, N. Rethinking pruning large language models: Benefits and pitfalls of reconstruction error minimization. June 2024. URL <https://arxiv.org/abs/2406.15524>.
- Sun, M., Liu, Z., Bair, A., and Kolter, J. Z. A simple and effective pruning approach for large language models. 2024. URL <https://openreview.net/forum?id=PxoFut3dWW>.
- Touvron, H., Martin, L., Stone, K., Albert, P., Almahairi, A., Babaei, Y., Bashlykov, N., Batra, S., Bhargava, P., Bhosale, S., Bikel, D., Blecher, L., Canton-Ferrer, C., Chen, M., Cucurull, G., Esiobu, D., Fernandes, J., Fu, J., Fu, W., Fuller, B., Gao, C., Goswami, V., 0001, N. G., Hartshorn, A., Hosseini, S., Hou, R., Inan, H., Kardas, M., Kerkez, V., Khabsa, M., Kloumann, I., Korenev, A., Koura, P. S., Lachaux, M.-A., Lavril, T., Lee, J., Liskovich, D., Lu, Y., Mao, Y., Martinet, X., Mihaylov, T., Mishra, P., Molybog, I., Nie, Y., Poulton, A., Reizenstein, J., Rungta, R., Saladi, K., Schelten, A., Silva, R., Smith, E. M., Subramanian, R., Tan, X. E., Tang, B., Taylor, R., Williams, A., Kuan, J. X., Xu, P., Yan, Z., Zarov, I., Zhang, Y., Fan, A., Kambadur, M., Narang, S., Rodriguez, A., Stojnic, R., Edunov, S., and Scialom, T. Llama 2: Open foundation and fine-tuned chat models. *CoRR*, abs/2307.09288, July 2023. doi: 10.48550/arxiv.2307.09288. URL <https://doi.org/10.48550/arxiv.2307.09288>.
- Wang, A., Singh, A., Michael, J., Hill, F., Levy, O., and Bowman, S. R. Glue: A multi-task benchmark and analysis platform for natural language understanding. *BlackboxNLP@EMNLP*, pp. 353–355, April 2018. doi: 10.18653/v1/w18-5446. URL <https://doi.org/10.18653/v1/w18-5446>.
- Wang, P., Fan, Z., Hu, S., 0024, Z. C., 0001, Y. W., and 0027, Y. W. Reconstruct the pruned model without any retraining. *CoRR*, abs/2407.13331, 2024. doi: 10.48550/arxiv.2407.13331. URL <https://doi.org/10.48550/arxiv.2407.13331>.
- Wu, H. Llm-bip: Structured pruning for large language models with block-wise forward importance propagation. *CoRR*, abs/2412.06419, 2024. doi: 10.48550/arxiv.2412.06419. URL <https://doi.org/10.48550/arxiv.2412.06419>.
- Xiao, G., Lin, J., Seznec, M., Wu, H., Demouth, J., and Han, S. Smoothquant: Accurate and efficient post-training quantization for large language models. In *International conference on machine learning*, pp. 38087–38099. PMLR, 2023. URL <https://proceedings.mlr.press/v202/xiao23c/xiao23c.pdf>.
- Xiao, Q., Ansell, A., Wu, B., 0006, L. Y., Pechenizkiy, M., 0003, S. L., and Mocanu, D. C. Leave it to the specialist: Repair sparse llms with sparse fine-tuning via sparsity evolution. *CoRR*, abs/2505.24037, 2025. doi: 10.48550/arxiv.2505.24037. URL <https://doi.org/10.48550/arxiv.2505.24037>.
- Xu, P., Shao, W., Chen, M., Tang, S., Zhang, K., Gao, P., An, F., Qiao, Y., and Luo, P. Besa: Pruning large language models with blockwise parameter-efficient sparsity allocation. In *The Twelfth International Conference on Learning Representations*. URL <https://openreview.net/forum?id=gC6JTEU3jl>.
- Yang, A., Yang, B., Hui, B., 0007, B. Z., 0002, B. Y., 0005, C. Z., 0001, C. L., Li, C., Liu, D., 0005, F. H., Dong, G., Wei, H., Lin, H., Tang, J., Wang, J., 0003, J. Y., Tu, J., 0012, J. Z., Ma, J., Yang, J., Xu, J., 0001, J. Z., Bai, J., He, J., Lin, J., Dang, K., Lu, K., Chen, K., 0002, K. Y., Li, M., Xue, M., Ni, N., 0011, P. Z., 0028, P. W., Peng, R., Men, R., Gao, R., Lin, R., 0007, S. W., Bai, S., Tan, S., Zhu, T., Li, T., 0001, T. L., Ge, W., Deng, X., Zhou, X., Ren, X., 0017, X. Z., Wei, X., Ren, X., Liu, X., Fan, Y., Yao, Y., Zhang, Y., 0004, Y. W., Chu, Y., Liu, Y., Cui, Z., Zhang, Z., Guo, Z., and Fan, Z. Qwen2 technical report. *CoRR*, abs/2407.10671, 2024. doi: 10.48550/arxiv.2407.10671. URL <https://doi.org/10.48550/arxiv.2407.10671>.
- Yin, L., Wu, Y., Zhang, Z., Hsieh, C.-Y., Wang, Y., Jia, Y., Li, G., Jaiswal, A. K., Pechenizkiy, M., Liang, Y., Bendersky, M., Wang, Z., and Liu, S. Outlier weighed layerwise sparsity (OWL): A missing secret sauce for pruning LLMs to high sparsity. In Salakhutdinov, R., Kolter, Z., Heller, K., Weller, A., Oliver, N., Scarlett, J., and Berkenkamp, F. (eds.), *Proceedings of the 41st International Conference on Machine Learning*, volume 235 of *Proceedings of Machine Learning Research*, pp. 57101–57115. PMLR, 21–27 Jul 2024. URL <https://proceedings.mlr.press/v235/yin24e.html>.
- Zellers, R., Holtzman, A., Bisk, Y., Farhadi, A., and 0001, Y. C. Hellaswag: Can a machine really finish your sentence? *ACL*, pp. 4791–4800, May 2019. doi: 10.18653/v1/p19-1472. URL <https://doi.org/10.18653/v1/p19-1472>.
- Zhang, S., Roller, S., Goyal, N., Artetxe, M., Chen, M., Chen, S., Dewan, C., Diab, M., Li, X., Lin, X. V., Mihaylov, T., Ott, M., Shleifer, S., Shuster, K., Simig, D., Koura, P. S., Sridhar, A., Wang, T., and Zettlemoyer, L. Opt: Open pre-trained transformer language models. 2022. URL <https://arxiv.org/abs/2205.01068>.
- Zhang, Y., Bai, H., Lin, H., Zhao, J., Hou, L., and Canistraci, C. V. Plug-and-play: An efficient post-training

pruning method for large language models. In *The Twelfth International Conference on Learning Representations*, 2024. URL <https://openreview.net/forum?id=Tr0lPx9woF>.

Zhao, P., Hu, H., Li, P., Zheng, Y., Wang, Z., and Yuan, X. A convex-optimization-based layer-wise post-training pruner for large language models. *CoRR*, 2024. URL <https://openreview.net/forum?id=KXMBY8PA9I>.

Zimmer, M., Andoni, M., Spiegel, C., and Pokutta, S. Perp: Rethinking the prune-retrain paradigm in the era of llms. 2025. URL <https://arxiv.org/abs/2312.15230>.

A. Additional Related Work Notes

Two adjacent directions are worth noting. First, several methods study *where* to place sparsity across a network (e.g., non-uniform sparsity allocation across layers/blocks) under a fixed global budget (Xu et al.; Wu, 2024; An et al., 2024; Yin et al., 2024). Second, sparse training methods maintain sparsity throughout training by dynamically updating connectivity patterns (Bellec et al., 2018; Mocanu et al., 2018; Mostafa & Wang, 2019; Dettmers & Zettlemoyer, 2019; Evcı et al., 2020; Liu et al., 2020). These methods study different objectives and settings than the ones of post-training local reconstruction and introduce additional confounders (e.g., varying where sparsity is placed), so we leave them out of scope and focus on reconstruction after post-training pruning.

B. Loss Function and Propagation Strategy

Propagation: How to define inputs and targets? Pruning a model locally involves splitting it into submodels and sequentially pruning each submodel. Before discussing the different propagation strategies, recall the pruning objective in Equation 2 and let us specify how the input activations \mathbf{X} for the submodel f we want to prune are computed. We denote by $\mathbf{X} := f_0(\mathbf{X}_0; \theta_0)$ the output of the submodel f_0 consisting of all layers prior to f with parameters θ_0 based on input data \mathbf{X}_0 . Further, we denote by $\hat{\mathbf{X}} := f_0(\mathbf{X}_0; \hat{\theta}_0)$ the output of the submodel f_0 using the pruned weights $\hat{\theta}_0$. The different propagation strategies are defined by whether we use calibration inputs $\hat{\mathbf{X}}$ or \mathbf{X} , and similarly, whether to align the outputs with $f(\mathbf{X}; \theta)$ or $f(\hat{\mathbf{X}}; \theta)$. We outline three distinct strategies:

1. **Dense Propagation (DP):** Both inputs and targets are sourced from the original dense model, i.e., the objective is $\min_{\hat{\theta}} \|f(\mathbf{X}; \hat{\theta}) - f(\mathbf{X}; \theta)\|_F^2$. Here, the pruned submodel is reconstructed to best match the dense one, ignoring the error caused by pruning the prior submodels.
2. **Sparse Propagation (SP):** Inputs come from the pruned model and targets are generated by further processing the sparse inputs through the dense model, i.e., the objective is $\min_{\hat{\theta}} \|f(\hat{\mathbf{X}}; \hat{\theta}) - f(\hat{\mathbf{X}}; \theta)\|_F^2$. This approach is consistent with the EBFT method (Guo et al., 2024), where the reconstruction objective takes into account the error caused by pruning the prior submodels.
3. **Mixed Propagation (MP):** Inputs come from the pruned model, while targets are sourced from the dense model, i.e., the objective is $\min_{\hat{\theta}} \|f(\hat{\mathbf{X}}; \hat{\theta}) - f(\mathbf{X}; \theta)\|_F^2$. This approach tries to correct for the error caused by pruning the prior submodels by steering the activations to those of the dense model. (Shin et al., 2024) refer to this strategy as *global propagation*.

Loss: How to measure reconstruction quality? The loss function measures the similarity between the outputs of the reconstructed submodel and the target activations. We consider two loss functions: Mean Squared Error (MSE), the squared Euclidean distance averaged over batches; and Cosine Similarity (CS), a well-known measure of similarity between latent representations in NLP.

Table 6, Table 5, Table 7, and Table 8 show the results of the different propagation strategies and loss functions for OPT-1.3B, OPT-6.7B, LLaMA-2-13B, and LLaMA-3-8B, respectively. Overall, we observe no systematic difference between the different propagation strategies and loss functions; both in terms of perplexity and zero-shot accuracy. Notably, for both OPT-1.3B and OPT-6.7B, finer granularities are not only on par with coarser granularities, but often better by a significant margin.

A Free Lunch in LLM Compression: Revisiting Retraining after Pruning

Table 5. Perplexity and zero-shot accuracy of OPT-6.7B pruned to different sparsity types with Wanda and reconstructed in different settings with 1024 calibration samples. The best result for each setting is underlined, the best result for each sparsity type is highlighted in bold. SP, MP, DP: sparse, mixed, and dense propagation. CS: cosine similarity. ↓: lower is better, ↑: higher is better. Base perplexity of OPT-6.7B dense: 10.86, pruned unstructured: 12.06, pruned 2:4: 16.05.

Sparsity type	Block size	Perplexity ↓						Zero-shot accuracy (in %) ↑					
		SP		MP		DP		SP		MP		DP	
		MSE	CS	MSE	CS	MSE	CS	MSE	CS	MSE	CS	MSE	CS
50% unstructured	1/2	11.51	11.36	11.48	11.37	11.51	11.36	49.94	50.08	<u>50.38</u>	50.47	50.08	50.24
	1	11.64	11.63	11.92	11.88	11.58	11.69	49.92	<u>50.62</u>	50.03	50.20	49.82	50.52
	2	11.59	11.54	11.75	11.91	11.61	11.53	<u>49.97</u>	<u>50.60</u>	50.28	50.04	49.90	50.63
	8	11.85	11.89	11.89	11.95	11.84	11.90	49.84	49.76	50.03	49.90	49.76	49.78
2:4	1/2	13.41	13.01	<u>12.96</u>	12.72	13.40	12.93	47.71	48.24	<u>48.92</u>	48.94	47.67	48.35
	1	13.75	13.08	13.77	13.56	13.55	13.22	47.70	<u>48.77</u>	48.31	48.75	47.82	<u>48.76</u>
	2	<u>13.30</u>	<u>12.93</u>	13.38	13.39	13.42	<u>12.85</u>	<u>47.99</u>	<u>48.29</u>	48.53	48.76	<u>47.94</u>	48.66
	8	13.49	13.45	13.56	13.57	13.54	13.45	47.93	48.14	48.07	48.28	47.86	48.09

Table 6. Perplexity and zero-shot accuracy of OPT-1.3B pruned to different sparsity types with Wanda and reconstructed in different settings with 1024 calibration samples. The best result for each setting is underlined, the best result for each sparsity type is highlighted in bold. SP, MP, DP: sparse, mixed, and dense propagation. CS: cosine similarity. ↓: lower is better, ↑: higher is better. Base perplexity of OPT-1.3B dense: 14.62, pruned unstructured: 18.31, pruned 2:4: 28.11.

Sparsity type	Block size	Perplexity ↓						Zero-shot accuracy (in %) ↑					
		SP		MP		DP		SP		MP		DP	
		MSE	CS	MSE	CS	MSE	CS	MSE	CS	MSE	CS	MSE	CS
50% unstructured	1/2	<u>15.60</u>	<u>15.45</u>	15.47	15.43	15.60	15.45	44.99	45.16	<u>44.63</u>	<u>44.99</u>	44.68	45.02
	1	16.01	15.86	16.42	16.52	16.07	16.12	44.03	44.63	44.08	44.32	44.11	44.78
	2	16.03	15.81	16.26	16.34	16.03	15.78	43.86	44.47	44.26	44.27	44.00	44.49
	6	16.12	16.17	16.17	16.25	16.14	16.20	44.38	44.35	44.27	44.41	44.51	44.29
	12	16.20	16.34	16.19	16.28	16.22	16.38	43.99	44.02	44.11	44.33	44.26	44.03
	24	16.29	16.44	16.29	16.42	16.31	16.43	44.24	44.34	44.22	44.38	44.32	44.27
2:4	1/2	18.49	17.96	17.67	<u>17.82</u>	18.52	18.04	43.39	43.39	44.09	44.17	43.50	43.56
	1	19.39	18.41	19.37	19.74	19.67	18.94	42.67	<u>43.53</u>	42.97	43.27	42.66	<u>43.64</u>
	2	19.33	18.50	18.96	19.25	19.37	18.45	42.52	43.34	42.82	43.08	42.41	43.23
	6	19.28	19.21	19.25	19.38	19.37	19.23	42.76	43.30	43.17	43.14	42.88	43.42
	12	19.49	19.47	19.38	19.43	19.56	19.59	43.09	42.57	43.26	42.98	42.90	42.77
	24	19.76	19.85	19.73	19.81	19.76	19.84	43.02	42.92	43.04	42.84	42.94	42.88

Table 7. Perplexity and zero-shot accuracy of LLaMA-2-13B (40 transformer blocks) pruned to different sparsity types with Wanda and reconstructed in different settings with 1024 calibration samples. The best result for each setting is underlined, the best result for each sparsity type is highlighted in bold. SP, MP, DP: sparse, mixed, and dense propagation. CS: cosine similarity. ↓: lower is better, ↑: higher is better. Base perplexity of LLaMA-2-13B dense: 4.57, pruned unstructured: 5.54, pruned 2:4: 8.39.

Sparsity type	Block size	Perplexity ↓						Zero-shot accuracy (in %) ↑					
		SP		MP		DP		SP		MP		DP	
		MSE	CS	MSE	CS	MSE	CS	MSE	CS	MSE	CS	MSE	CS
unstructured	1/2	5.33	5.33	5.26	5.33	5.34	5.35	60.53	60.84	60.99	60.96	60.59	60.59
	1	5.32	5.35	5.26	5.34	5.33	5.37	<u>61.18</u>	<u>61.03</u>	<u>61.25</u>	61.30	61.02	60.75
	2	5.32	5.36	<u>5.27</u>	5.33	5.33	5.37	60.93	60.45	60.91	<u>60.84</u>	60.62	60.61
	10	<u>5.30</u>	<u>5.31</u>	5.29	<u>5.30</u>	<u>5.31</u>	<u>5.33</u>	60.94	60.99	61.09	61.01	<u>61.06</u>	<u>60.95</u>
2:4	1/2	6.76	6.80	6.24	6.59	6.71	6.80	56.16	56.15	58.66	58.30	56.34	56.10
	1	6.68	6.72	6.32	6.63	6.67	6.79	56.42	56.47	58.75	<u>58.52</u>	56.61	<u>56.45</u>
	2	6.56	6.64	6.35	6.52	6.60	6.73	55.94	56.35	57.81	58.38	<u>56.93</u>	56.33
	10	<u>6.37</u>	<u>6.37</u>	6.33	<u>6.35</u>	<u>6.39</u>	<u>6.42</u>	<u>56.64</u>	<u>56.70</u>	57.03	56.82	<u>56.36</u>	56.36

A Free Lunch in LLM Compression: Revisiting Retraining after Pruning

Table 8. Perplexity and zero-shot accuracy of LLaMA-3-8B (32 transformer blocks) pruned to different sparsity types with Wanda and reconstructed in different settings with 1024 calibration samples. The best result for each setting is underlined, the best result for each sparsity type is highlighted in bold. SP, MP, DP: sparse, mixed, and dense propagation. CS: cosine similarity. ↓: lower is better, ↑: higher is better. Base perplexity of LLaMA-3-8B dense: 5.83, pruned unstructured: 8.96, pruned 2:4: 21.58.

Sparsity type	Block size	Perplexity ↓						Zero-shot accuracy (in %) ↑					
		SP		MP		DP		SP		MP		DP	
		MSE	CS	MSE	CS	MSE	CS	MSE	CS	MSE	CS	MSE	CS
unstructured	1/2	7.99	8.00	7.75	7.99	7.84	7.99	<u>57.57</u>	<u>57.54</u>	<u>58.81</u>	57.44	58.80	57.64
	1	7.76	8.00	7.70	7.92	7.75	8.02	<u>58.55</u>	<u>57.77</u>	<u>58.08</u>	58.45	58.84	57.66
	2	<u>7.75</u>	7.98	7.72	<u>7.79</u>	<u>7.74</u>	8.02	58.31	<u>58.39</u>	58.21	<u>58.67</u>	58.29	<u>58.20</u>
	8	<u>7.82</u>	<u>7.89</u>	7.86	<u>7.83</u>	<u>7.83</u>	<u>7.95</u>	58.07	<u>57.94</u>	57.86	58.04	58.10	<u>57.76</u>
	16	8.06	7.99	8.06	7.96	8.02	8.03	57.26	57.48	57.41	57.76	57.16	57.53
2:4	1/2	15.79	15.28	9.96	11.96	11.36	12.78	46.91	47.58	<u>55.74</u>	50.71	51.18	49.66
	1	11.14	12.60	10.34	11.84	10.95	12.67	<u>52.48</u>	50.99	54.55	55.77	<u>52.65</u>	50.55
	2	10.74	11.90	10.34	11.18	10.56	12.04	52.00	51.24	52.78	53.33	51.51	50.16
	8	<u>10.44</u>	<u>10.59</u>	10.57	<u>10.59</u>	<u>10.52</u>	<u>10.88</u>	52.47	<u>52.51</u>	52.92	53.44	52.40	<u>51.77</u>
	16	11.10	10.90	11.18	10.92	11.11	11.02	51.81	52.07	51.83	52.55	51.16	51.60

C. Using MiniPile as a Calibration Set

Table 9 shows perplexity and zero-shot accuracy of LLaMA-3-8B when pruned and reconstructed with a subset of MiniPile (Kaddour, 2023) as calibration data. Comparing the results to Table 8, we see that 1) the overall performance of the reconstructed models improves slightly when using MiniPile instead of C4, and 2) the relative performance differences between granularities, loss functions, and propagation strategies stay close to identical.

Table 9. Perplexity and zero-shot accuracy of LLaMA-3-8B (32 transformer blocks) pruned to different sparsity types with Wanda and reconstructed in different settings with 1024 calibration samples from the MiniPile dataset. The best result for each setting is underlined, the best result for each sparsity type is highlighted in bold. SP, MP, DP: sparse, mixed, and dense propagation. CS: cosine similarity. ↓: lower is better, ↑: higher is better. Base perplexity of LLaMA-3-8B dense: 5.83, pruned unstructured: 8.96, pruned 2:4: 21.58.

Sparsity type	Block size	Perplexity ↓						Zero-shot accuracy (in %) ↑					
		SP		MP		DP		SP		MP		DP	
		MSE	CS	MSE	CS	MSE	CS	MSE	CS	MSE	CS	MSE	CS
unstructured	1/2	7.85	7.98	7.68	7.89	7.84	7.98	<u>59.72</u>	59.27	<u>60.40</u>	61.04	59.77	59.16
	1	7.73	7.92	7.68	7.83	7.72	7.94	59.31	<u>59.55</u>	60.04	60.23	59.90	59.40
	2	<u>7.69</u>	7.88	7.66	<u>7.72</u>	7.69	7.92	59.16	59.39	59.52	60.25	59.17	59.39
	8	<u>7.71</u>	<u>7.77</u>	7.75	7.72	7.72	<u>7.83</u>	58.81	58.87	59.00	59.15	58.68	58.59
	16	8.03	7.97	7.90	7.82	7.91	7.87	57.62	57.86	58.08	58.33	57.86	58.16
2:4	1/2	11.48	12.77	9.65	10.75	11.16	12.33	53.18	51.16	<u>56.50</u>	56.66	53.23	51.05
	1	10.95	12.35	9.69	10.70	10.65	12.21	<u>54.28</u>	52.10	56.31	56.60	<u>54.11</u>	51.88
	2	10.60	11.58	10.26	10.83	10.44	11.57	52.73	51.69	54.05	55.18	53.06	51.02
	8	<u>10.15</u>	<u>10.25</u>	10.35	<u>10.29</u>	<u>10.23</u>	<u>10.55</u>	53.32	<u>53.49</u>	53.87	54.06	53.12	<u>52.42</u>
	16	11.82	10.46	10.82	10.52	10.77	10.61	50.24	52.00	52.80	53.48	52.27	52.29

D. Effect of Reconstruction on Structured Pruning

In this section, we investigate how reconstruction affects structured pruning. As a baseline, we consider FLAP (An et al., 2024), a structured pruning method that non-uniformly distributes sparsity across transformer blocks to achieve superior performance. We compare the performance of Wanda-sp, a structured pruning method that uniformly distributes sparsity across transformer blocks based on Wanda (Sun et al., 2024), with and without reconstruction to FLAP. Table 10 shows that reconstruction after structured pruning with Wanda-sp significantly improves the performance of Wanda-sp, to the point that it outperforms the non-uniformly distributed sparsity of FLAP.

Table 10. Perplexity and zero-shot accuracy of LLaMA-2-7B when pruned with structured Wanda (Wanda-sp) and FLAP. The reconstruction after pruning with Wanda-sp is performed with 1024 calibration samples and block size 1.

Sparsity	Perplexity			Zero-shot accuracy		
	FLAP	Wanda-sp no rec.	Wanda-sp rec.	FLAP	Wanda-sp no rec.	Wanda-sp rec.
20%	7.81	8.61	7.76	53.42%	54.40%	56.09%
50%	46.25	57.77	30.97	42.87%	36.05%	44.24%

E. Additional Experiments on Granularity

Together with Table 6, Table 5, Table 7, and Table 8 in Appendix B, we present additional experiments ablating the effect of granularity on the final model quality. Additionally, Table 11, Table 12 compare per-matrix reconstruction with multiple coarser granularities under different loss functions and propagation strategies. One clear trend is that per-matrix reconstruction heavily underperforms in the mixed propagation setting. Hence, Table 13 and Table 14 compare per-matrix reconstruction using sparse propagation with block-wise reconstruction using mixed propagation (our default setting).

Overall, the trend observed in section 3 persists. Apart from per-matrix reconstruction, the final model quality is either largely insensitive to granularity or even slightly worse for coarser granularities and smaller models.

Table 11. Perplexity and zero-shot accuracy of OPT-1.3B pruned to different sparsity types with Wanda and reconstructed in different settings with 1024 calibration samples. The best result for each setting is underlined, the best result for each sparsity type is highlighted in bold. SP, MP, DP: sparse, mixed, and dense propagation. CS: cosine similarity. ↓: lower is better, ↑: higher is better. Base perplexity of OPT-1.3B dense: 14.62, pruned unstructured: 18.31, pruned 2:4: 28.11.

Sparsity type	Block size	Perplexity ↓						Zero-shot accuracy (in %) ↑					
		SP		MP		DP		SP		MP		DP	
		MSE	CS	MSE	CS	MSE	CS	MSE	CS	MSE	CS	MSE	CS
50% unstructured	Per-matrix	17.31	17.88	21.74	22.01	18.41	18.32	44.13	43.70	42.54	42.47	43.42	43.56
	1/2	<u>15.53</u>	<u>15.46</u>	<u>15.47</u>	15.44	<u>15.59</u>	<u>15.46</u>	44.80	45.32	<u>44.86</u>	<u>45.03</u>	<u>44.94</u>	<u>45.29</u>
	1	16.02	15.91	16.42	16.54	16.09	16.13	44.16	44.80	44.05	44.30	44.27	44.91
	2	16.03	15.82	16.25	16.35	16.04	15.80	43.94	44.40	44.27	44.28	44.00	44.55
	6	16.12	16.17	16.17	16.25	16.14	16.20	44.47	44.36	44.30	44.19	44.45	44.34
2:4	Per-matrix	24.48	26.25	42.62	46.41	27.96	27.69	41.84	41.08	40.35	40.86	41.44	41.84
	1/2	<u>18.50</u>	<u>18.02</u>	<u>17.77</u>	<u>17.85</u>	<u>18.59</u>	<u>18.09</u>	43.34	43.42	<u>44.04</u>	44.26	<u>43.21</u>	<u>43.57</u>
	1	19.72	18.42	19.40	19.78	19.86	18.92	42.73	<u>43.52</u>	43.54	43.18	42.76	<u>43.63</u>
	2	19.15	18.47	18.99	19.22	19.38	18.41	42.59	43.41	42.90	43.15	42.38	43.16
	6	19.33	19.24	19.48	19.71	19.41	19.26	42.75	43.09	42.63	42.66	42.89	43.41

Table 12. Perplexity and zero-shot accuracy of OPT-6.7B pruned to different sparsity types with Wanda and reconstructed at various granularities and 1024 calibration samples. Layer norm parameters are fixed for comparability with per-matrix reconstruction. The best result for each setting is underlined, the best result for each sparsity type is highlighted in bold. ↓: lower is better, ↑: higher is better. Dense baseline: 10.86 perplexity, pruned unstructured: 12.06, pruned 2:4: 16.05.

Sparsity type	Block size	Perplexity ↓						Zero-shot accuracy (in %) ↑					
		SP		MP		DP		SP		MP		DP	
		MSE	CS	MSE	CS	MSE	CS	MSE	CS	MSE	CS	MSE	CS
unstructured	Per-matrix	11.55	11.72	98.15	49.72	11.96	11.99	49.39	49.48	43.64	44.95	48.78	48.98
	1/2	11.49	11.27	11.66	11.34	11.51	11.40	49.99	50.62	50.60	50.49	49.86	50.14
	1	11.65	11.59	11.95	11.90	11.56	11.71	49.85	50.54	49.97	50.27	49.86	50.61
	2	11.61	11.56	11.78	11.84	11.60	11.57	<u>50.02</u>	50.52	50.23	50.18	<u>49.92</u>	50.62
	8	11.84	11.90	11.86	11.91	11.88	11.93	49.73	49.75	50.02	49.89	49.84	49.68
2:4	Per-matrix	14.25	15.82	293.26	104.03	16.06	15.52	47.02	46.94	38.42	40.62	45.53	45.99
	1/2	13.39	12.98	<u>12.97</u>	12.72	13.45	12.97	47.87	48.18	48.90	48.80	47.84	48.28
	1	<u>13.29</u>	13.04	13.85	13.58	13.59	13.21	47.91	<u>48.61</u>	48.31	48.59	47.84	<u>48.76</u>
	2	13.43	<u>12.93</u>	13.46	13.40	<u>13.41</u>	<u>12.90</u>	47.83	48.47	48.48	48.78	<u>48.03</u>	48.75
	8	13.47	13.51	13.52	13.55	13.64	13.24	<u>47.92</u>	47.98	48.35	48.31	47.82	48.25

A Free Lunch in LLM Compression: Revisiting Retraining after Pruning

Table 13. Perplexity and average zero-shot accuracy of different LLaMA-2 models when pruned and reconstructed in different settings. The calibration set size is 256 and the pruning method is Wanda. Sparsities 50% and 60% are unstructured. The best result for each model, reconstruction mode, prune method combination is highlighted in bold. ↓: lower is better, ↑: higher is better.

Perplexity ↓		7B (4.86)			13B (4.42)			70B (-)		
Method	Sparsity	No Rec.	Per-matrix	Block size 1	No Rec.	Per-matrix	Block size 1	No Rec.	Per-matrix	Block size 1
Magnitude	50%	12.77	6.70	6.12	6.05	5.52	5.28	4.71	3.85	3.69
SparseGPT	50%	6.13	6.11	5.92	5.48	5.37	5.25	3.81	3.79	3.71
Wanda	50%	6.05	6.02	5.86	5.37	5.29	5.18	3.69	3.66	3.58
Magnitude	60%	1370.12	14.44	8.08	9.58	8.41	6.43	7.93	5.16	4.40
SparseGPT	60%	8.37	8.24	7.11	7.14	7.10	6.31	4.86	4.81	4.70
Wanda	60%	8.97	8.79	7.08	7.37	7.22	6.21	4.75	4.72	4.52
Magnitude	2:4	36.09	11.33	10.06	7.37	7.30	7.04	6.23	6.21	4.60
SparseGPT	2:4	9.14	9.12	7.01	7.62	7.58	6.39	5.22	5.18	4.79
Wanda	2:4	9.90	9.86	6.98	7.71	7.59	6.22	5.02	5.01	4.56
Magnitude	4:8	12.97	8.21	6.63	6.41	6.25	5.87	5.34	5.28	4.12
SparseGPT	4:8	7.10	7.02	6.47	6.38	6.27	5.77	4.51	4.45	4.30
Wanda	4:8	7.28	7.17	6.36	6.25	6.21	5.71	4.24	4.19	4.08
Accuracy ↑		7B (59.70%)			13B (63.04%)			70B (-)		
Method	Sparsity	No Rec.	Per-matrix	Block size 1	No Rec.	Per-matrix	Block size 1	No Rec.	Per-matrix	Block size 1
Magnitude	50%	51.12%	54.90%	55.95%	52.82%	59.45%	60.42%	59.81%	65.63%	65.88%
SparseGPT	50%	56.44%	56.48%	56.71%	59.82%	60.26%	60.91%	66.19%	66.08%	66.48%
Wanda	50%	56.03%	56.08%	56.14%	60.34%	60.40%	60.98%	66.18%	66.20%	66.51%
Magnitude	60%	40.11%	46.88%	51.76%	43.91%	44.74%	55.78%	55.26%	63.35%	63.88%
SparseGPT	60%	51.78%	51.92%	52.52%	56.46%	56.92%	58.03%	64.87%	64.89%	65.12%
Wanda	60%	49.75%	50.28%	53.25%	56.20%	56.43%	58.02%	63.75%	63.81%	63.99%
Magnitude	2:4	47.47%	48.90%	49.02%	49.85%	52.02%	53.46%	58.87%	59.02%	63.12%
SparseGPT	2:4	51.57%	50.92%	52.97%	55.92%	55.96%	57.86%	62.47%	62.56%	63.67%
Wanda	2:4	48.61%	49.17%	52.36%	53.67%	54.15%	56.49%	62.86%	63.14%	63.84%
Magnitude	4:8	50.68%	52.42%	53.73%	52.81%	55.96%	57.31%	59.32%	59.39%	64.72%
SparseGPT	4:8	53.91%	54.22%	54.33%	58.64%	59.49%	59.67%	64.75%	64.86%	65.16%
Wanda	4:8	52.54%	53.03%	54.67%	58.23%	58.30%	58.53%	65.06%	65.11%	65.14%

Table 14. Perplexity and average zero-shot accuracy of different Qwen-2.5-Instruct models when pruned and reconstructed in different settings. The calibration set size is 256 and the pruning method is Wanda. Sparsities 50% and 60% are unstructured. The best result for each model, reconstruction mode, prune method combination is highlighted in bold. ↓: lower is better, ↑: higher is better.

Perplexity ↓		7B (5.16)			14B (2.39)			32B (2.19)			72B (1.88)		
Method	Sparsity	No Rec.	Per-matrix	Block size 1	No Rec.	Per-matrix	Block size 1	No Rec.	Per-matrix	Block size 1	No Rec.	Per-matrix	Block size 1
Magnitude	50%	568.93	9.92	7.94	18.27	8.12	7.71	13.22	4.90	4.36	444.81	4.34	4.28
SparseGPT	50%	7.59	7.47	7.41	6.68	6.59	6.55	4.84	4.81	4.69	4.20	4.17	4.03
Wanda	50%	7.67	7.52	7.40	6.42	6.38	6.12	4.43	4.42	4.25	3.70	3.64	3.65
Magnitude	60%	25551.15	31.35	12.35	60343.74	967.78	10.75	49.04	9.00	6.31	1071.23	7.80	6.02
SparseGPT	60%	13.33	11.97	9.60	117.86	50.59	9.69	6.62	6.60	6.47	6.38	6.29	6.22
Wanda	60%	26.51	15.64	9.29	170.16	76.10	9.23	62.11	7.02	6.28	5.78	5.68	5.70
Magnitude	2:4	5974.84	15.31	10.18	1424.70	387.53	12.11	38.34	67.16	6.31	226.30	6.88	5.93
SparseGPT	2:4	13.02	12.77	9.69	198.16	89.20	10.87	7.11	7.04	6.71	6.83	6.74	6.39
Wanda	2:4	15.98	15.19	9.60	242.79	58.58	12.85	37.52	13.89	6.50	5.99	5.96	5.86
Magnitude	4:8	4138.65	53.75	8.81	87.93	68.21	7.85	24.51	6.04	5.46	195.85	5.72	4.75
SparseGPT	4:8	8.95	8.76	8.21	56.11	35.51	7.12	6.10	5.86	5.88	5.42	5.40	5.33
Wanda	4:8	9.43	9.32	8.20	72.05	28.38	7.07	5.79	5.79	5.47	4.91	4.87	4.82
Accuracy ↑		7B (67.53%)			14B (71.05%)			32B (69.66%)			72B (72.32%)		
Method	Sparsity	No Rec.	Per-matrix	Block size 1	No Rec.	Per-matrix	Block size 1	No Rec.	Per-matrix	Block size 1	No Rec.	Per-matrix	Block size 1
Magnitude	50%	46.87%	63.30%	64.50%	61.56%	67.41%	67.55%	61.94%	67.52%	68.28%	51.27%	70.86%	71.16%
SparseGPT	50%	64.42%	65.22%	65.31%	68.75%	68.89%	68.94%	68.42%	68.42%	69.06%	71.25%	71.42%	71.76%
Wanda	50%	62.95%	64.01%	64.88%	68.36%	68.52%	68.76%	68.03%	68.42%	68.72%	70.94%	71.53%	71.72%
Magnitude	60%	35.41%	57.85%	60.58%	50.38%	63.34%	64.62%	55.24%	65.77%	67.05%	46.27%	68.15%	69.31%
SparseGPT	60%	60.23%	61.53%	62.40%	65.48%	65.37%	65.74%	66.14%	66.56%	66.98%	69.75%	70.02%	70.22%
Wanda	60%	60.67%	61.77%	62.00%	63.87%	64.66%	65.30%	66.09%	66.29%	67.30%	68.99%	69.78%	70.18%
Magnitude	2:4	41.23%	60.13%	61.52%	53.83%	61.22%	65.02%	58.55%	65.93%	67.32%	51.07%	68.21%	69.03%
SparseGPT	2:4	60.81%	60.97%	61.63%	64.76%	64.87%	65.63%	66.33%	66.38%	67.26%	69.20%	69.39%	69.44%
Wanda	2:4	59.18%	60.07%	61.52%	63.75%	64.49%	65.68%	66.41%	67.10%	67.39%	69.31%	69.99%	69.94%
Magnitude	4:8	44.65%	55.16%	63.34%	58.70%	60.18%	66.51%	59.47%	67.17%	68.13%	52.22%	69.38%	69.61%
SparseGPT	4:8	62.58%	63.21%	63.80%	67.14%	67.16%	67.76%	67.35%	67.78%	68.06%	69.96%	70.16%	70.92%
Wanda	4:8	61.61%	62.67%	62.96%	65.59%	66.32%	66.93%	67.54%	68.29%	68.53%	69.82%	70.41%	70.54%

F. Additional Experiments with Qwen-2.5-Instruct Models

Table 15 presents additional experiments with Qwen-2.5-Instruct models.

Table 15. Perplexity and average zero-shot accuracy of different Qwen-2.5-Instruct models when pruned and reconstructed in different settings. The calibration set size is 256 and the pruning method is Wanda. Sparsities 50% and 60% are unstructured. The best result for each model, reconstruction mode, sparsity combination is highlighted in bold. ↓: lower is better, ↑: higher is better.

Perplexity ↓		500M (12.01)		3B (7.52)		7B (5.16)		14B (2.39)		32B (2.19)		72B (1.88)	
Method	Sparsity	No Rec.	Rec.										
Magnitude	50%	2640.98	45.26	155.54	10.50	568.93	7.94	18.27	7.71	13.22	4.36	444.81	4.28
SparseGPT	50%	18.15	15.19	10.69	10.18	7.59	7.41	6.68	6.55	4.84	4.69	4.20	4.03
Wanda	50%	20.48	15.10	10.81	9.77	7.67	7.40	6.42	6.12	4.43	4.25	3.70	3.65
Magnitude	60%	13676.54	143.29	14787.87	15.37	25551.15	12.35	60343.74	10.75	49.04	6.31	1071.23	6.02
SparseGPT	60%	31.05	20.12	15.61	12.79	13.33	9.60	117.86	9.69	6.62	6.47	6.38	6.22
Wanda	60%	270.85	20.12	21.80	12.67	26.51	9.29	170.16	9.23	62.11	6.28	5.78	5.70
Magnitude	2:4	21017.80	31.35	27844.06	23.07	5974.84	10.18	1424.70	12.11	38.34	6.31	226.30	5.93
SparseGPT	2:4	28.16	19.54	16.17	12.92	13.02	9.69	198.16	10.87	7.11	6.71	6.83	6.39
Wanda	2:4	65.86	20.48	22.10	12.59	15.98	9.60	242.79	12.85	37.52	6.50	5.99	5.86
Magnitude	4:8	48867.85	135.66	31798.92	19.24	4138.65	8.81	87.93	7.85	24.51	5.46	195.85	4.75
SparseGPT	4:8	21.46	17.18	12.72	11.33	8.95	8.21	56.11	7.12	6.10	5.88	5.42	5.33
Wanda	4:8	34.23	17.42	14.90	11.22	9.43	8.20	72.05	7.07	5.79	5.47	4.91	4.82
Accuracy ↑		500M (49.56%)		3B (63.26%)		7B (67.53%)		14B (71.05%)		32B (69.66%)		72B (72.32%)	
Method	Sparsity	No Rec.	Rec.										
Magnitude	50%	37.33%	43.20%	39.82%	58.40%	46.87%	64.50%	61.56%	67.55%	61.94%	68.28%	51.27%	71.16%
SparseGPT	50%	44.05%	44.20%	55.68%	58.32%	64.42%	65.31%	68.75%	68.94%	68.42%	69.06%	71.25%	71.76%
Wanda	50%	41.87%	45.23%	58.98%	60.99%	62.95%	64.88%	68.36%	68.76%	68.03%	68.72%	70.94%	71.72%
Magnitude	60%	33.14%	41.05%	33.72%	54.31%	35.41%	60.58%	50.38%	64.62%	55.24%	67.05%	46.27%	69.31%
SparseGPT	60%	40.63%	42.11%	52.28%	54.18%	60.23%	62.40%	65.48%	65.74%	66.14%	66.98%	69.75%	70.22%
Wanda	60%	39.27%	42.78%	50.22%	55.83%	60.67%	62.00%	63.87%	65.30%	66.09%	67.30%	68.99%	70.18%
Magnitude	2:4	33.28%	39.25%	32.28%	51.31%	41.23%	61.52%	53.83%	65.02%	58.55%	67.32%	51.07%	69.03%
SparseGPT	2:4	38.53%	42.85%	52.90%	55.38%	60.81%	61.63%	64.76%	65.63%	66.33%	67.26%	69.20%	69.44%
Wanda	2:4	36.76%	43.08%	48.31%	55.29%	59.18%	61.52%	63.75%	65.68%	66.41%	67.39%	69.31%	69.94%
Magnitude	4:8	32.88%	41.60%	32.49%	52.29%	44.65%	63.34%	58.70%	66.51%	59.47%	68.13%	52.22%	69.61%
SparseGPT	4:8	41.99%	43.88%	54.86%	57.85%	62.58%	63.80%	67.14%	67.76%	67.35%	68.06%	69.96%	70.92%
Wanda	4:8	41.33%	44.08%	55.30%	59.64%	61.61%	62.96%	65.59%	66.93%	67.54%	68.53%	69.82%	70.54%

G. Hyperparameters

Here, we provide the hyperparameters used for local reconstruction, full retraining, and MaskLoRA fine-tuning.

Table 16. Hyperparameters used for local reconstruction, full retraining, and MaskLoRA fine-tuning.

Method	Learning rate	Warmup ratio	Scheduler	Number of epochs	Optimizer
Local reconstruction	{1e-6, 5e-6, 1e-5, 5e-5, 1e-4}	0.1	Linear	{1, 5, 10}	AdamW
MaskLoRA fine-tuning	{5e-7, 1e-6, 5e-6, 1e-5, 5e-5, 1e-4, 5e-4, 1e-3}	0.1	Linear	{1, 5, 10}	AdamW
Full retraining	{5e-7, 1e-6, 5e-6, 1e-5, 5e-5, 1e-4, 5e-4, 1e-3}	0.1	Linear	{1, 5, 10}	AdamW
Method	Batch size	Gradient accumulation	LoRA rank	LoRA alpha	Max. gradient norm
Local reconstruction	2	1	-	-	-
MaskLoRA fine-tuning	1	2	16	32	{0.5, 1.0, 1.5}
Full retraining	1	2	-	-	{0.5, 1.0, 1.5}